Supplementary Information

Effect of *tert*-butyl groups on electronic communication between redox units in tetrathiafulvalene-tetraazapyrene triads

Ping Zhou,[a] Ulrich Aschauer,[a] Silvio Decurtins,[a] Thomas Feurer,[b] Robert Häner[a] and Shi-Xia Liu*[a]

[a] *Department of Chemistry, Biochemistry and Pharmaceutical Sciences, University of Bern, Freiestrasse 3, CH-3012 Bern, Switzerland. E-mail: shi-xia.liu@unibe.ch*
[b] *Institute of Applied Physics, University of Bern, Sidlerstrasse 5, CH-3012 Bern, Switzerland*

Experimental Section

General

Air- and/or water-sensitive reactions were conducted under nitrogen and dry, freshly distilled solvents were used. Chemicals used for the synthesis of the compounds were purchased from commercial suppliers (Sigma-Aldrich, TCI or Alfa Aesar). UV-Vis-NIR absorption spectra were recorded on a Perkin Elmer Lambda 900 UV/Vis/NIR spectrometer and UV-Vis absorption spectra on a Varian Cary-100 Bio-UV/VIS. ^{1}H and ^{13}C NMR spectra were recorded on a Bruker Avance 300 or 400 spectrometer at 300 MHz and 75 MHz or 101 MHz, respectively. Chemical shifts are reported in parts per million (ppm) and are referenced to the residual solvent peak ($CDCl_3$, δ ^{1}H = 7.26 ppm, and DMSO-d_6, δ ^{1}H = 2.50 ppm). The following abbreviations were used s (singlet), d (doublet), t (triplet) and m (multiplet). High resolution mass spectra (HR-MS) were obtained on a Thermo Fisher LTQ Orbitrap XL using Nano Electrospray Ionization.

Cyclic voltammetry (CV) was performed in a three-electrode cell equipped with a Pt working electrode, a glassy carbon counter-electrode, and Ag/AgCl reference electrode. The electrochemical experiments were carried out under an oxygen-free atmosphere in dichloromethane with $TBAPF_6$ (0.1 M) as a supporting electrolyte. Naphthalene-1,4,5,8-tetraamine tin(II) salt (**1**)[1] and 4,5,9,10-tetrabromo-1,3,6,8-tetraazapyrene (**5**)[2] were prepared as described in the literature.

TTF-TAP. A mixture of compound **5** (52.2 mg, 0.1 mmol) and TTF precursor (**4**) (144 mg, 0.2 mmol) in anhydrous DMF (10 mL) was sonicated about 15 min. And then a solution of $CsOH{\cdot}H_2O$ (101 mg, 0.6 mmol) in anhydrous MeOH (5 mL) was dropwise added to the resultant solution over 1 h, forming an orange solution. After additional stirring for 4 h under N_2 at r.t., the reaction mixture was concentrated *in vacuo*. The residue was dissolved in CH_2Cl_2 and extracted with H_2O for three times. The combined organic phase was concentrated under reduced pressure and purified by column chromatography (silica gel, CH_2Cl_2:Hex = 1:1, v/v) to afford **TTF-TAP** as a yellow-green powder (25 mg, 18%). ^{1}H NMR (300 MHz, $CDCl_3$) δ 10.01 (s, 2H), 2.83 (t, J =

7.3 Hz, 8H), 1.66-1.59 (m, 8H), 1.41-1.19 (m, 56H), 0.89 (t, J = 6.5 Hz, 12H). MALDI-TOF-MS (*m/z*): calcd for $[C_{64}H_{86}N_4S_{16}]^+$ 1422.24; found: 1422.53. HR-MS (ESI, positive): *m/z* calcd for $[C_{64}H_{86}N_4S_{16}]^+$ 1422.2378; found: 1422.2416; calcd for $[C_{64}H_{86}N_4S_{16}]^{2+}$ 711.1186; found: 711.1206. Elemental analysis (%) calcd for $C_{64}H_{86}N_4S_{16}$: C, 53.97; H, 6.09; N, 3.93; found: C, 54.46; H, 6.22; N, 3.98.

***t*-Bu-TAP (2)**. To a suspension of 1,4,5,8-tetraaminonaphthalene hexachlorostannate (**1**) (0.25 g, 0.48 mmol) in dry THF (10 mL) was added an excess of absolute triethylamine (2 mL) under N_2. Pivalic anhydride (2 mmol, 0.4 mL) was added slowly to the reaction mixture and kept in an ice cooling bath. The reaction mixture was then refluxed for 48 h. After cooling down to room temperature, the solvent was removed under reduced pressure, and the residue was purified by column chromatography (silica, hexane/CH_2Cl_2 4:1, v/v) to afford **2** as a light-yellow powder (92 mg, 60%). ^{1}H NMR (300 MHz, $CDCl_3$) δ 8.54 (s, 4H), 1.67 (s, 18H). ^{13}C NMR (75 MHz, $CDCl_3$) δ 176.72, 152.59, 136.03, 112.06, 40.66, 30.46. HR-MS (ESI, positive): *m/z* calcd for $[C_{20}H_{22}N_4+H]^+$ 319.1917; found: 319.1908.

tetrabromo-*t*-Bu-TAP (3). ***t*-Bu-TAP** (**2**) (285 mg, 0.9 mmol) was dissolved in concentrated sulfuric acid (30 mL). Iodine (39 mg, 0.15 mmol) and bromine (0.45 mL, 8.7 mmol) were added. The reaction mixture was heated to 80 °C for 3 h, and then allowed to cool to room temperature and stirred overnight. The mixture was poured on ice, neutralized with a saturated aqueous solution of NaOH, and extracted with $CHCl_3$. The solvent was removed under reduced pressure, and the residue was purified by column chromatography (silica, hexane/CH_2Cl_2 4:1, v/v) to afford **3** as a light-yellow powder (400 mg, 70%). ^{1}H NMR (300 MHz, $CDCl_3$) δ 1.71 (s, 18H). ^{13}C NMR (101 MHz, $CDCl_3$) δ 178.58, 151.41, 136.47, 110.67, 41.40, 30.29. HR-MS (ESI, positive): *m/z* calcd for $[C_{20}H_{18}Br_4N_4+H]^+$ 630.8338; found: 630.8326.

TTF-*t*-Bu-TAP. A mixture of compound **3** (50.7 mg, 0.08 mmol) and TTF precursor (**4**) (115 mg, 0.16 mmol) in anhydrous DMF (10 mL) was sonicated about 15 min. To the resulting solution was dropwise added a solution of $CsOH\cdot H_2O$ (81 mg, 0.48 mmol) in anhydrous MeOH (5 mL) over 1 h, forming an orange solution. After additional stirring for 4 h under N_2 at r.t., the reaction mixture was concentrated *in vacuo*. The residue was dissolved in CH_2Cl_2 and extracted with H_2O. The combined green organic phase was concentrated under reduced pressure and purified by column chromatography (silica gel, CH_2Cl_2:Hex = 1:2, v/v) to afford the pure product as a light-green powder (30 mg, 24%). ^{1}H NMR (300 MHz, $CDCl_3$) δ 2.83 (t, J = 7.4 Hz, 8H), 1.69-1.60 (m, 26H), 1.33-1.23 (m, 56H), 0.88 (t, J = 6.7 Hz, 12H). MALDI-TOF-MS (*m/z*): calcd for $[C_{72}H_{102}N_4\ S_{16}+H]^+$ 1535.37; found: 1535.87. HR-MS (ESI, positive): *m/z* calcd for $[C_{72}H_{102}N_4S_{16}]_2^{2+}$ 1534.3630; found: 1534.3663; calcd for $[C_{72}H_{102}N_4\ S_{16}]^{2+}$ 767.1812; found: 767.1832. Elemental analysis (%) calcd for $C_{72}H_{102}N_4S_{16}$: C, 56.28; H, 6.69; N, 3.65; found: C, 56.28; H, 6.77; N, 3.66.

Table S1 Electrochemical data, energies of HOMO and LUMO, and HOMO-LUMO gaps of two triads and precursors. Redox potentials (*V*) *vs* Ag/AgCl in CH_2Cl_2.

Compound	$E^{OX1}_{1/2}$ (V)	$E^{OX2}_{1/2}$ (V)	$E^{OX3}_{1/2}$ (V)	$E^{red1}_{1/2}$ (V)	$E^{red2}_{1/2}$ (V)	HOMO (eV)	LUMO (eV)	E_g (eV)
TTF-TAP	0.63	0.77	1.04	-0.48	-0.98	-4.87	-3.90	0.97
TTF-*t*-Bu-TAP	0.70	1.03		-0.67	-1.21	-4.89	-3.67	1.22
***t*-Bu-TAP**				-1.03			-3.32	
TTF precursor **4**	0.65	0.99				-4.86		

$E_{LUMO} = -e\ (E^{onset}_{red} + 4.29)$, $E_{HOMO} = -e\ (E^{onset}_{ox} + 4.29)$, E^{onset}_{red} = the onset reduction potentials, E^{onset}_{ox} = the onset oxidation potentials, $E_{HOMO} = E_{LUMO} - E_g$, Fc/Fc^+ is 0.51 V relative to Ag/AgCl in CH_2Cl_2.

Differential pulse voltammetry (DPV) measurements of two triads (Figure S1) were carried out, clearly showing that the two TTF units of **TTF-TAP** are sequentially oxidized to the TTF radical cation species while this process occurs simultaneously in **TTF-*t*-Bu-TAP**.

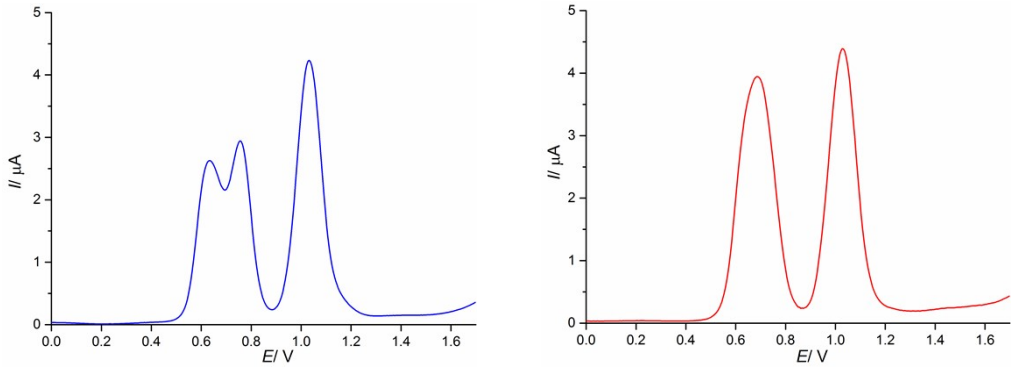

Figure S1: Differential pulse voltammograms of **TTF-TAP** a) and **TTF-*t*-Bu-TAP** b) at the concentration of 3×10^{-4} M.

To get a good understanding of the distinct electrochemical behaviors of triads **TTF-TAP** and **TTF-*t-Bu*-TAP** in terms of the degree of aggregation impeded by the presence of bulky tert-butyl groups, we did perform concentration-dependent CVs of **TTF-TAP** (Fig. S2). The step-wise oxidations of **TTF-TAP** are observed even in a very diluted solution (Fig. S2). Furthermore, concentration-dependent UV-Vis spectra

of two triads (Figure S3) were carried out. In both cases, the absorbance is proportional to the concentration, suggesting that no strong intermolecular interactions occur. Based on all these results, the possibility of associations between **TTF-TAP** molecules is definitively ruled out.

a)

b)

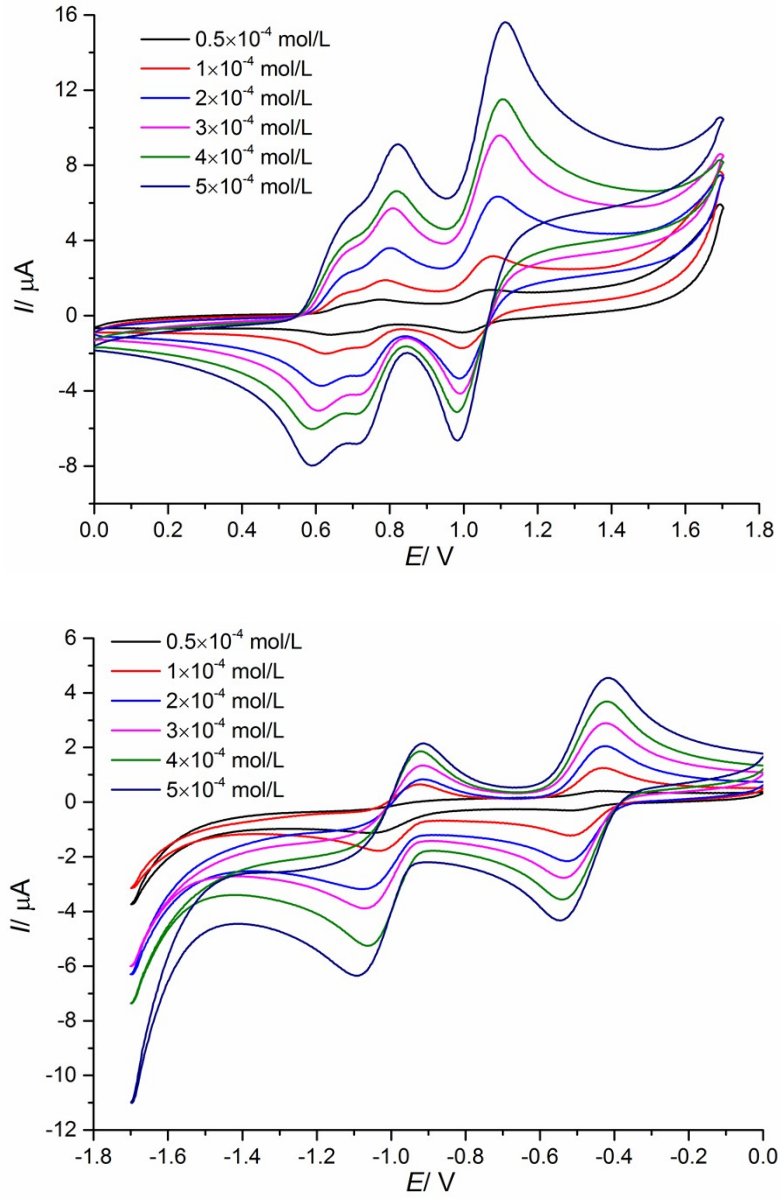

Figure S2: Cyclic voltammograms of **TTF-TAP** as a function of concentration in the positive a) and negative b) potential windows.

a)

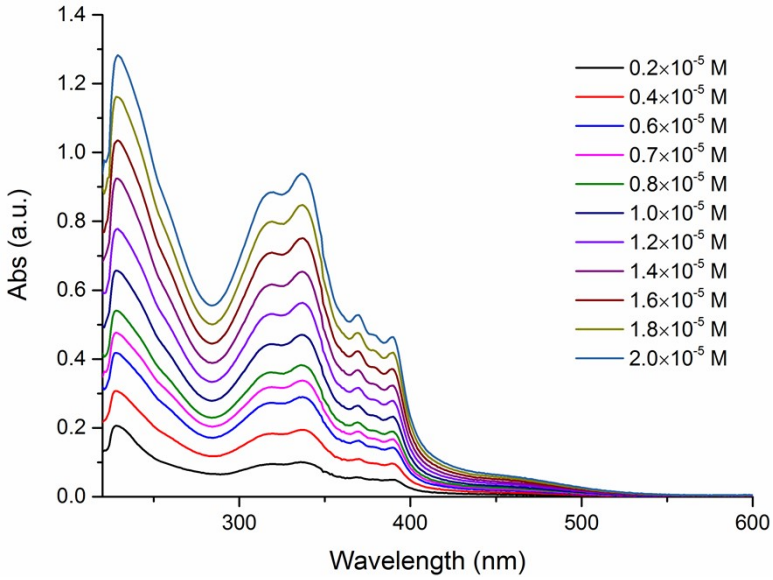

b)

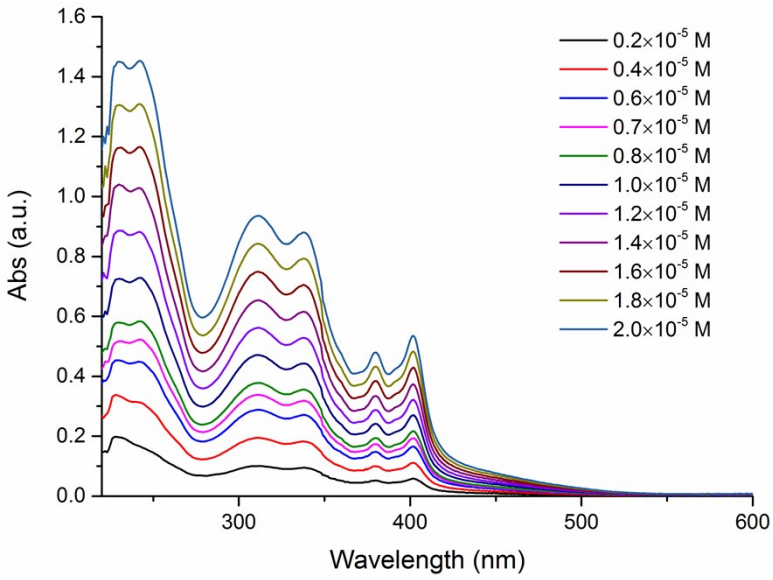

Figure S3: Concentration-dependent UV-Vis spectra of a) **TTF-TAP** and b) **TTF-*t*-Bu-TAP**.

Figure S4 shows the optimized structure of the **TTF-TAP** and **TTF-*t*-Bu-TAP** triads. Both structures have a planar TAP core with curved TTF moieties attached at an angle *via* the sulfur atoms.

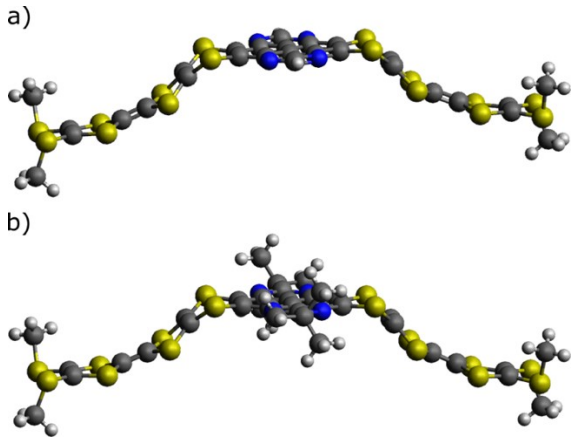

Figure S4: Structures of a) **TTF-TAP** and b) **TTF-*t*-Bu-TAP** triads.

Intuitively, energy levels of MOs change if non-zero partial charges are next to them. The LUMO is localized closer to where the *tert*-butyl groups are attached. Leaving aside electron rearrangement (which do not seem to happen comparing Fig. 5 and Fig. S3 and also from atomic charges), any electrostatic effect decays with 1/r going away from the attachment point. As a result, electrostatically the LUMO is more affected than the HOMO. Moreover, DFT calculations show that the insertion of *tert*-butyl groups leads to a slight decrease in electrostatic potentials at all nuclear positions (Table S2). This implies that electrons are in lower energy states around the nuclei dominating the LUMO and hence virtual orbitals (without electrons) become destabilized.

Table S2. The electrostatic potentials (in atomic units) at nuclear positions (see attached figure for atom numbering).

Atom	**TTF-TAP**	**TTF-*t*-Bu-TAP**	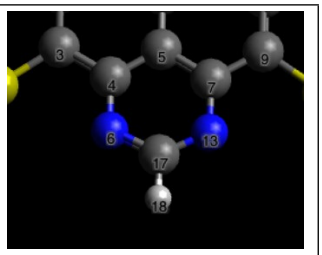
3	-14.656914	-14.662298	
4	-14.647453	-14.654592	
5	-14.687975	-14.696912	
6	-18.328110	-18.338104	
17	-14.645921	-14.650957	

The C17-C18 bond length is slightly shorter (1.530Å) than for example those in the *tert*-butyl itself (1.537Å and 1.547Å), indicative of hyperconjugation.

Figure S5 shows the adsorption spectra of the **TTF-TAP** and **TTF-*t*-Bu-TAP** triads obtained *via* TD-DFT calculations at the B3LYP/6-31G(d,p) level of theory. After DFT relaxation to within default thresholds, TD-DFT calculations of the lowest excited states were carried out and the absorption spectra extracted with GaussSum 3.0. As there are transitions with vanishing oscillator strength at large wavelengths, the 10 lowest energy transitions along with their oscillator strength and molecular orbital contributions are given in Tables S3 and S4.

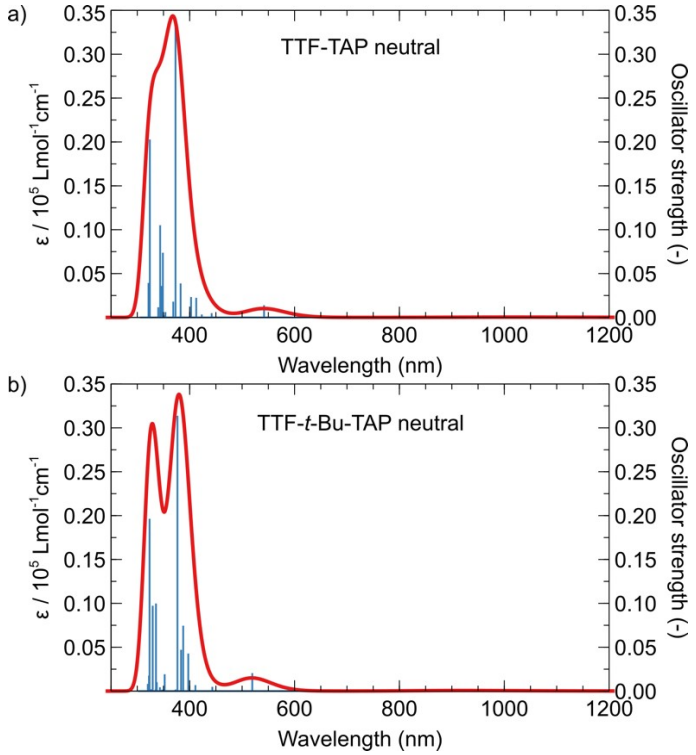

Figure S5: Computed absorption spectra and oscillator strengths of the charge neutral a) **TTF-TAP** and b) **TTF-*t*-Bu-TAP** triads.

Table S3: Computed transitions in the **TTF-TAP** triad.

Wavelength (nm)	**Oscillator strength**	**Molecular orbital contributions**			
1019.77458	0	HOMO	→	LUMO	(99%)
1014.18563	0.0005	HOMO-1	→	LUMO	(99%)
560.431194	0	HOMO-2	→	LUMO	(95%)
541.817913	0.0139	HOMO-3	→	LUMO	(97%)
473.583625	0	HOMO	→	LUMO+1	(99%)
473.457032	0.001	HOMO-1	→	LUMO+1	(99%)
441.869607	0.0049	HOMO-1	→	LUMO+4	(48%)
		HOMO	→	LUMO+3	(49%)
441.806624	0.0005	HOMO-1	→	LUMO+3	(48%)
		HOMO	→	LUMO+4	(49%)
423.00987	0.0002	HOMO-1	→	LUMO+2	(82%)
422.995439	0.0034	HOMO	→	LUMO+2	(90%)

Table S4: Computed transitions in the **TTF-*t*-Bu-TAP** triad.

Wavelength (nm)	**Oscillator strength**	**Molecular orbital contributions**			
926.430494	0	HOMO	→	LUMO	(98%)
921.473006	0.0009	HOMO-1	→	LUMO	(99%)
537.286328	0	HOMO-2	→	LUMO	(95%)
519.327272	0.0205	HOMO-3	→	LUMO	(97%)
443.101365	0.0049	HOMO-1	→	LUMO+3	(45%)
		HOMO	→	LUMO+4	(41%)
443.038031	0.0004	HOMO-1	→	LUMO+4	(46%)
		HOMO	→	LUMO+3	(40%)
435.337756	0	HOMO-8	→	LUMO	(37%)
		HOMO	→	LUMO+1	(56%)
435.184953	0	HOMO-1	→	LUMO+1	(90%)
435.108591	0.0007	HOMO-8	→	LUMO	(61%)
		HOMO	→	LUMO+1	(34%)
410.883821	0.0068	HOMO	→	LUMO+2	(93%)

Figure S6 shows the molecular orbitals involved in the main transitions of triads **TTF-TAP** and **TTF-*t*-Bu-TAP**. While the highest occupied orbitals represent different linear combinations of mainly TTF contributions, the LUMO is dominated by the TAP core.

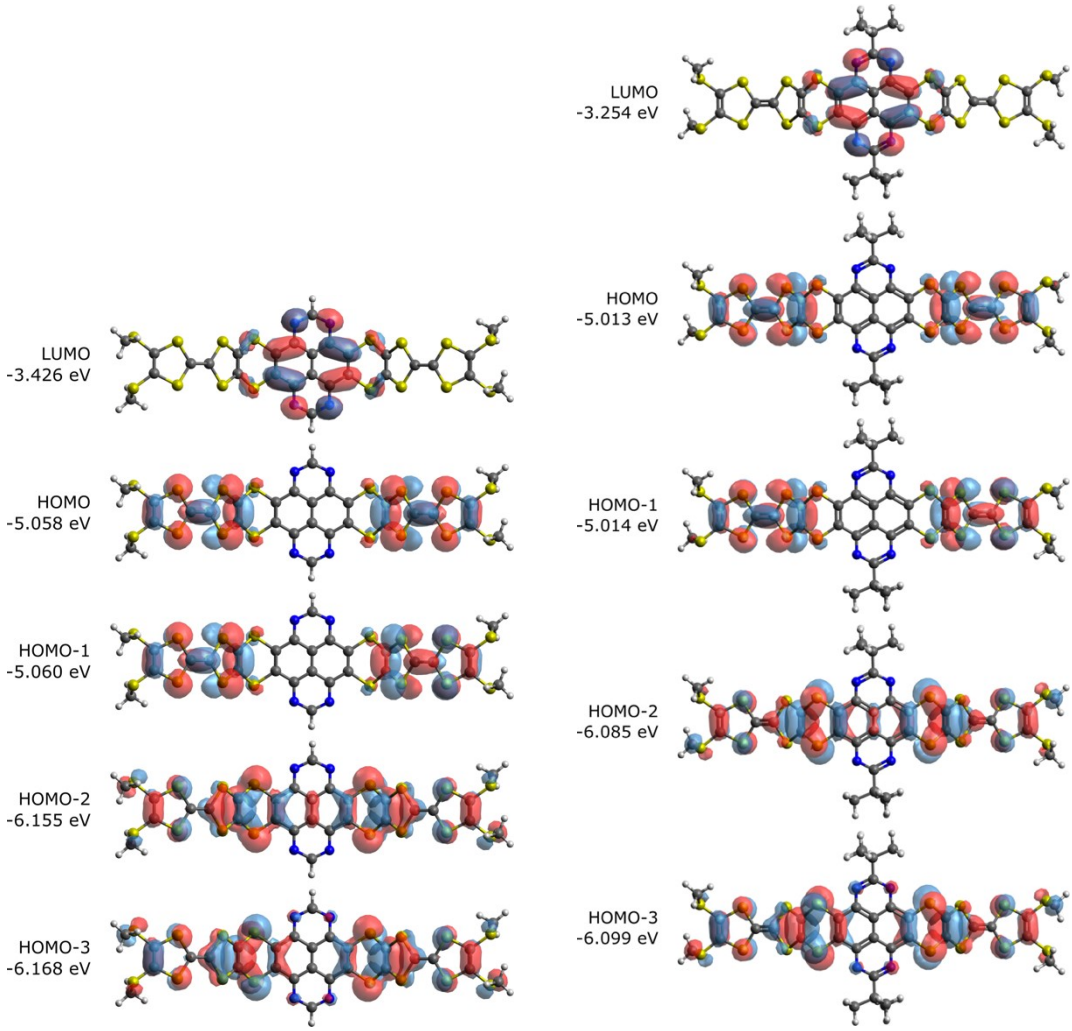

Figure S6: Molecular orbitals of **TTF-TAP** (left) and **TTF-*t*-Bu-TAP** (right) along with their molecular orbital energy.

Figure S7 shows the computed absorption spectra of the **TTF-TAP** and **TTF-*t*-Bu-TAP** triads in the cationic +1 and +2 charge states. For the +2 charge state a triplet configuration was found to be energetically favorable compared to the singlet case. In all cases transitions at wavelengths larger than 1000 nm become active. Tables S5-S8 give the main transitions (oscillator strength > 0.01) for the four cationic triads, while **Figures S8-S11** show the primarily involved molecular orbitals.

Importantly, the appearance of new absorptions at wavelengths above 400 nm is well represented, in good agreement with the optical spectra of the chemically oxidized triads. Thereby, the calculation for the open-shell +1 cationic state of the triads acts as a clarifying example for characterizing the occurrence of the intense broad NIR absorption, since two strong excitations $D_0 \rightarrow D_3$ (99% β-HOMO-2 to β-LUMO) and $D_0 \rightarrow D_4$ (99% β-HOMO-1 to β-LUMO) at 1013 nm and 1008 nm, respectively, lie in that spectral region. The involved molecular orbitals reveal that through photoexcitation, the majority of charge remains on the TTF units, but there is also some distinct charge flow from the central moiety towards the terminal parts. The absorptions in the 400 - 550 nm range are of mixed orbital nature.

Moreover, TD-DFT calculations in presence of a CH_2Cl_2 solvent modelled *via* the SMD implicit solvation model[3] show that the presence of the solvent has little effect on the absorption spectra of the neutral triads but blueshifts the main excitations of the cations by 100 to 200 nm for the +2 and +1 charge states respectively.

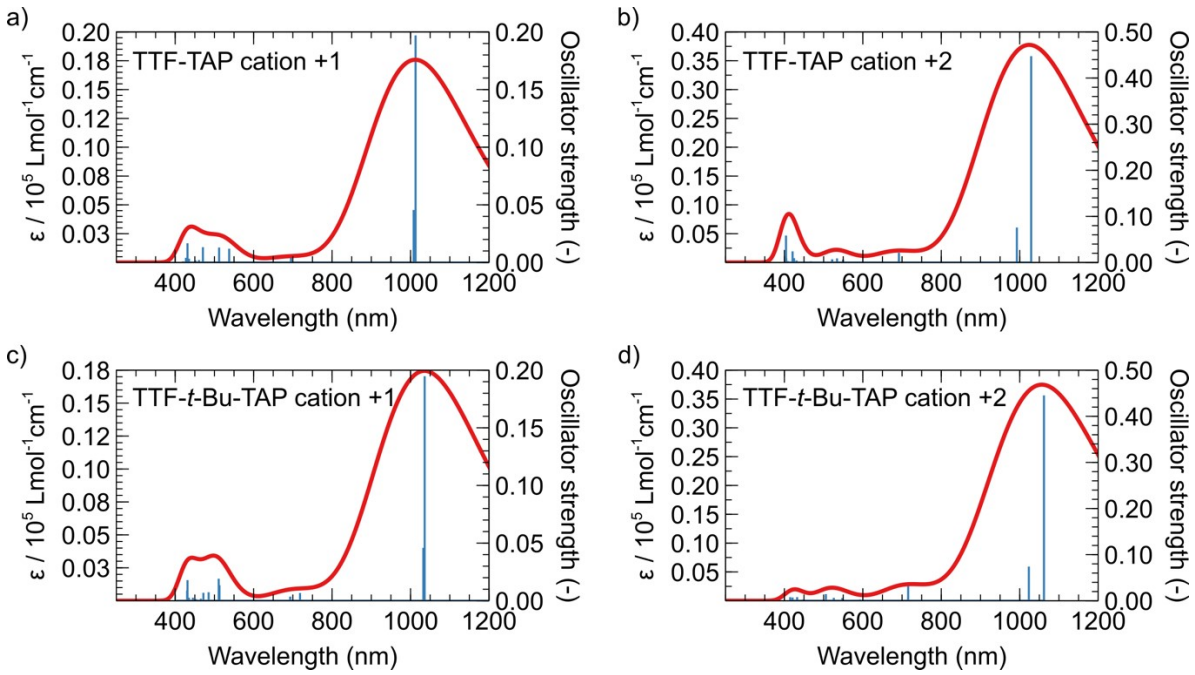

Figure S7: Computed absorption spectra of the cationic a) +1 **TTF-TAP**, b) +2 **TTF-TAP**, c) +1 **TTF-*t*-Bu-TAP** and d) +2 **TTF-*t*-Bu-TAP** triads.

Table S5: Computed transitions (oscillator strength > 0.01) in the cationic +1 **TTF-TAP** triad.

Wavelength (nm)	**Oscillator strength**	**Molecular orbital contributions**			
1012.86	0.197	HOMO-2(B)	→	LUMO(B)	99%
1007.91963	0.0456	HOMO-1(B)	→	LUMO(B)	99%
537.682436	0.012	HOMO-3(A)	→	LUMO(A)	45%
		HOMO-2(B)	→	LUMO+1(B)	47%
511.992868	0.013	HOMO-1(A)	→	LUMO+3(A)	33%
		HOMO(A)	→	LUMO+2(A)	33%
		HOMO(B)	→	LUMO+4(B)	23%
470.671145	0.0133	HOMO-9(B)	→	LUMO(B)	97%
431.399419	0.0167	HOMO-1(A)	→	LUMO+1(A)	11%
		HOMO-1(A)	→	LUMO+10(A)	14%
		HOMO(A)	→	LUMO+11(A)	13%
		HOMO(B)	→	LUMO+11(B)	27%

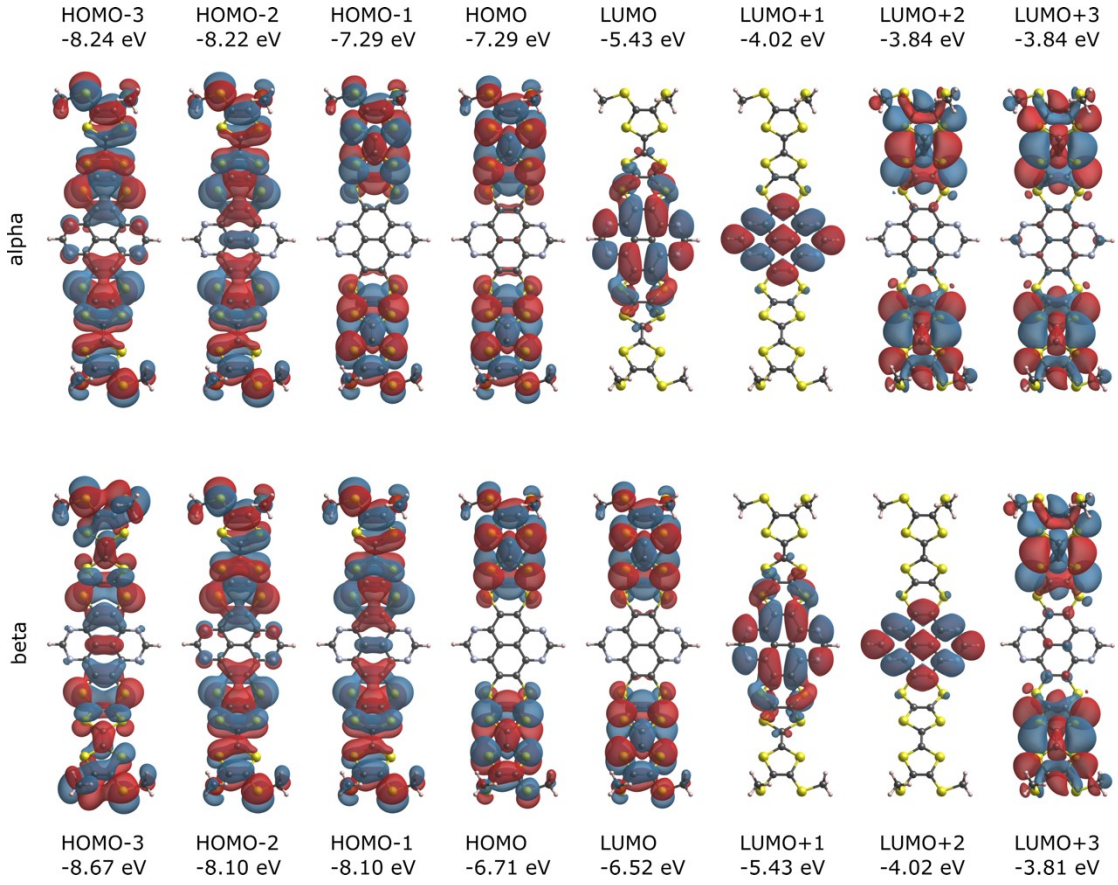

Figure S8: Primary molecular orbitals involved in the transitions of the cationic +1 **TTF-TAP** triad.

Table S6: Computed transitions (oscillator strength > 0.01) in the cationic +2 **TTF-TAP** triad.

Wavelength (nm)	**Oscillator strength**	**Molecular orbital contributions**			
1029.25613	0.4475	HOMO-1(B)	→	LUMO(B)	18%
		HOMO-1(B)	→	LUMO+1(B)	28%
		HOMO(B)	→	LUMO(B)	32%
		HOMO(B)	→	LUMO+1(B)	20%
992.747162	0.0759	HOMO-1(B)	→	LUMO(B)	30%
		HOMO-1(B)	→	LUMO+1(B)	17%
		HOMO(B)	→	LUMO(B)	19%
		HOMO(B)	→	LUMO+1(B)	34%
692.030548	0.021	HOMO-3(B)	→	LUMO(B)	37%
		HOMO-3(B)	→	LUMO+1(B)	12%
		HOMO-2(B)	→	LUMO(B)	46%
420.856052	0.0241	HOMO-11(B)	→	LUMO(B)	22%
		HOMO-9(B)	→	LUMO(B)	37%
404.199625	0.0585	HOMO-8(B)	→	LUMO(B)	41%
		HOMO-8(B)	→	LUMO+1(B)	41%

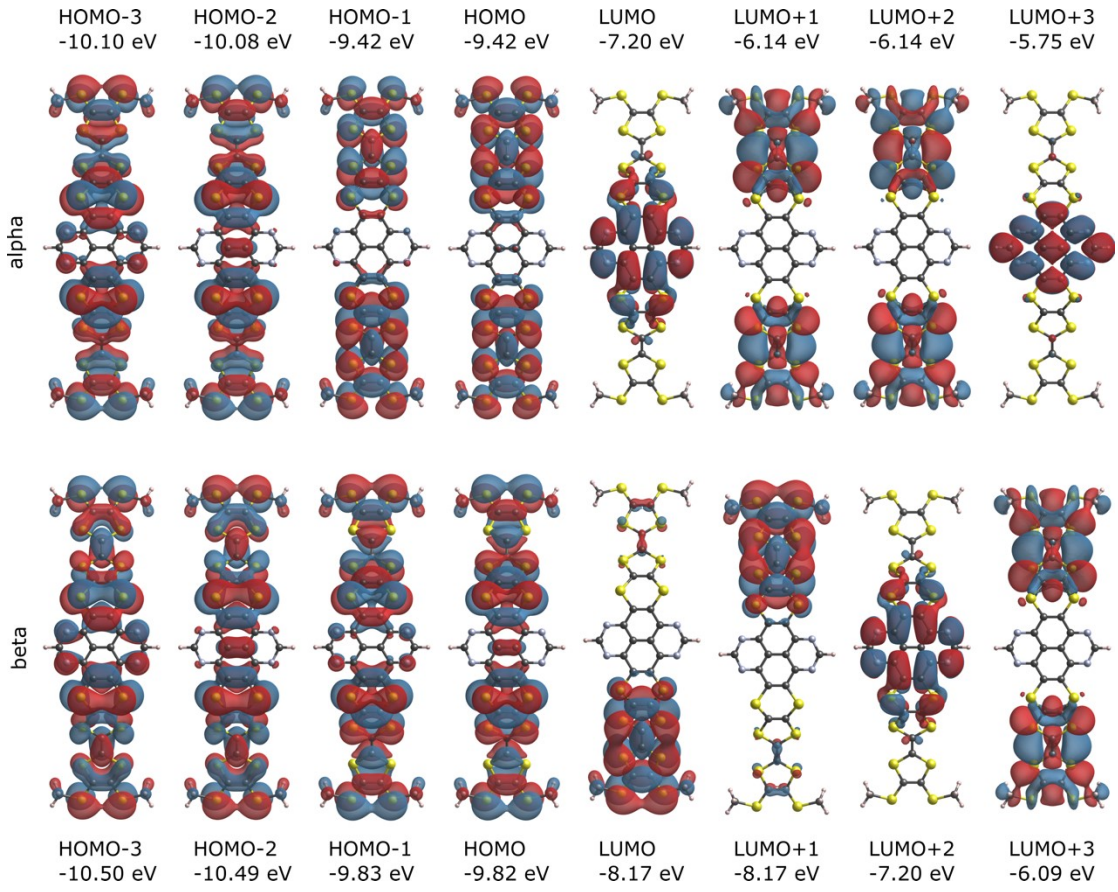

Figure S9: Primary molecular orbitals involved in the transitions of the cationic +2 **TTF-TAP** triad.

Table S7: Computed transitions (oscillator strength > 0.01) in the cationic +1 **TTF-*t*-Bu-TAP** triad.

Wavelength (nm)	**Oscillator strength**	**Molecular orbital contributions**			
1036.05075	0.1948	HOMO-2(B)	→	LUMO(B)	99%
1032.77129	0.0459	HOMO-1(B)	→	LUMO(B)	99%
512.924843	0.0135	HOMO-1(A)	→	LUMO+1(A)	36%
		HOMO(A)	→	LUMO+2(A)	37%
		HOMO(B)	→	LUMO+2(B)	24%
510.895801	0.0191	HOMO-3(A)	→	LUMO(A)	44%
		HOMO-2(B)	→	LUMO+1(B)	49%
431.444455	0.0179	HOMO-1(A)	→	LUMO+10(A)	15%
		HOMO(A)	→	LUMO+11(A)	13%
		HOMO-13(B)	→	LUMO(B)	23%
		HOMO(B)	→	LUMO+11(B)	31%

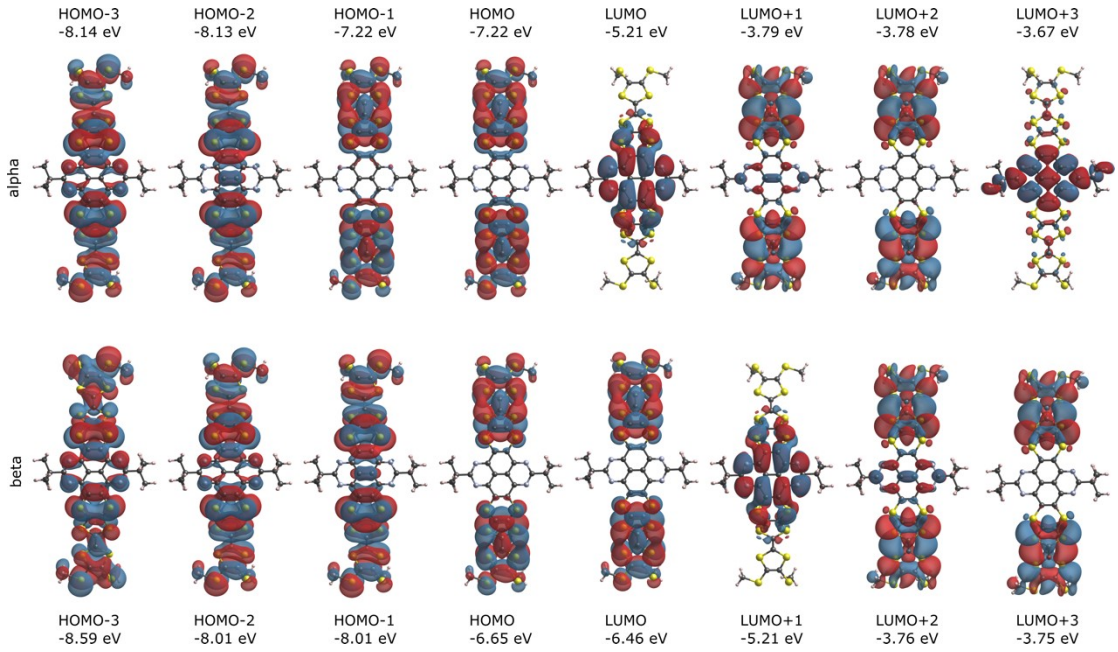

Figure S10: Primary molecular orbitals involved in the transitions of the cationic +1 **TTF-*t*-Bu-TAP** triad.

Table S8: Computed transitions (oscillator strength > 0.01) in the cationic +2 **TTF-*t*-Bu-TAP** triad.

Wavelength (nm)	**Oscillator strength**	**Molecular orbital contributions**			
1061.78122	0.4454	HOMO-1(B)	→	LUMO+1(B)	41%
		HOMO(B)	→	LUMO(B)	47%
1023.30962	0.0741	HOMO-1(B)	→	LUMO(B)	42%
		HOMO(B)	→	LUMO+1(B)	48%
715.596174	0.0329	HOMO-3(B)	→	LUMO(B)	48%
		HOMO-2(B)	→	LUMO(B)	12%
		HOMO-2(B)	→	LUMO+1(B)	38%
505.789553	0.0144	HOMO-3(A)	→	LUMO(A)	39%
		HOMO-1(B)	→	LUMO+2(B)	43%

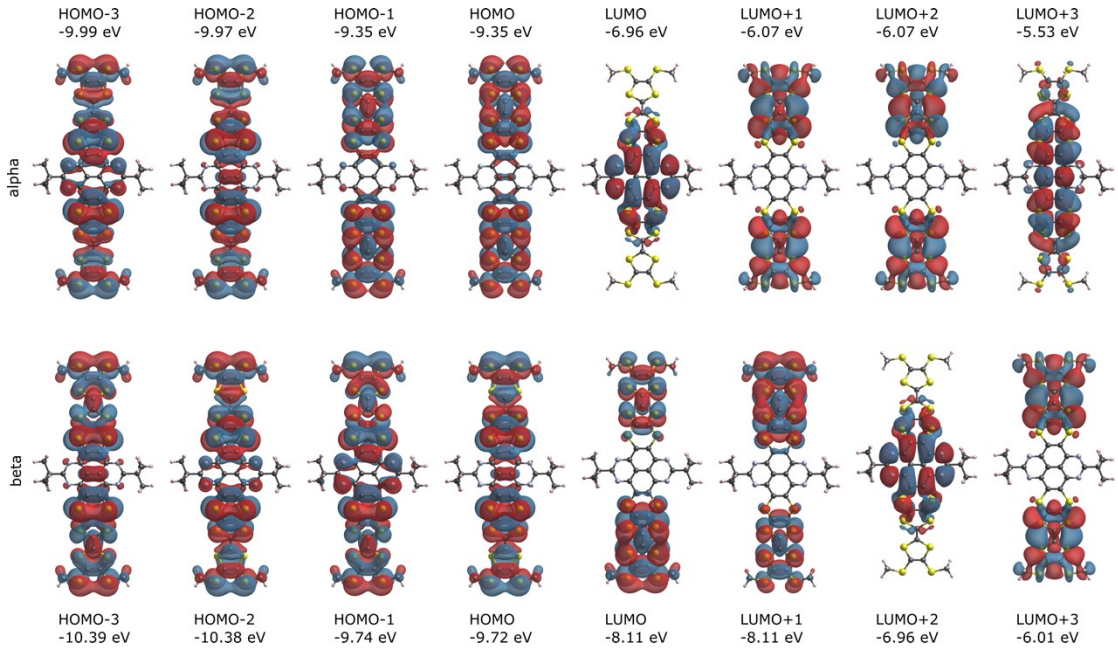

Figure S11: Primary molecular orbitals involved in the transitions of the cationic +2 **TTF-*t*-Bu-TAP** triad.

NMR and MS spectra

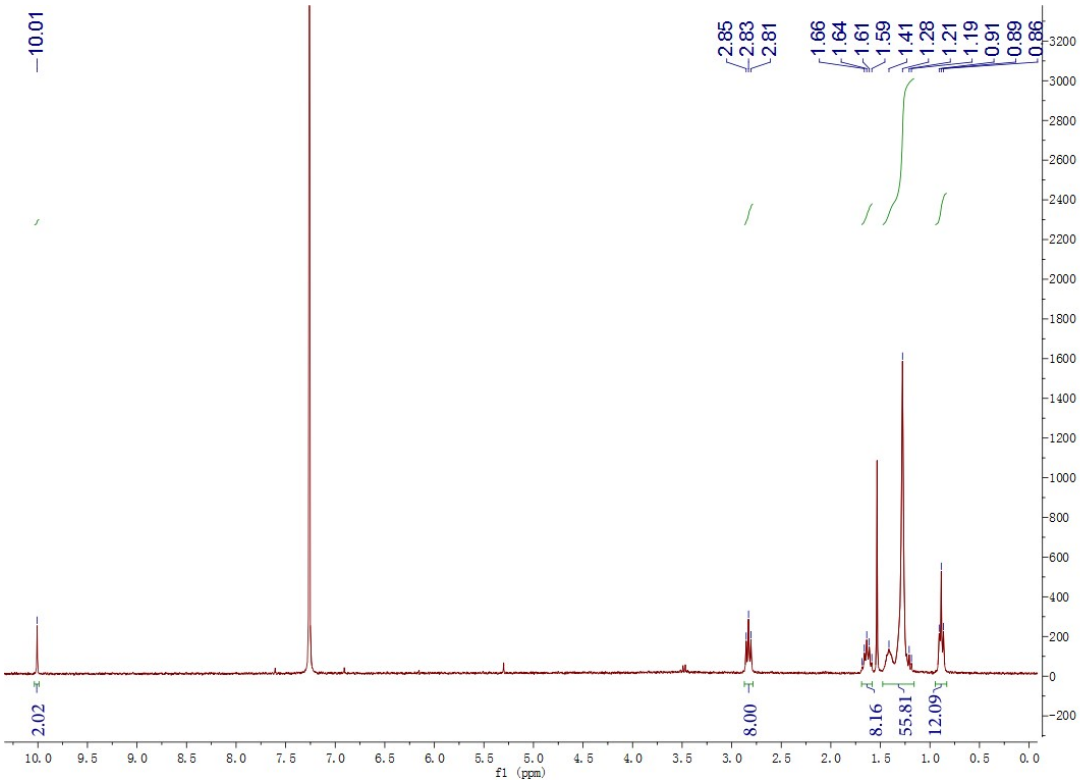

^{1}H NMR spectrum of **TTF-TAP** in $CDCl_3$.

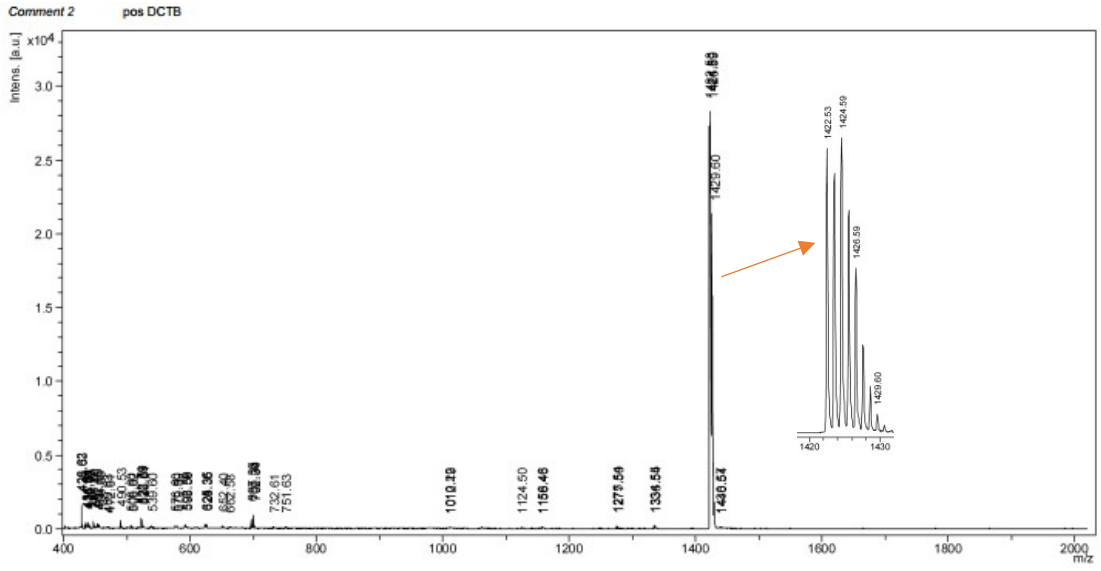

MALDI-TOF-MS analysis of **TTF-TAP**.

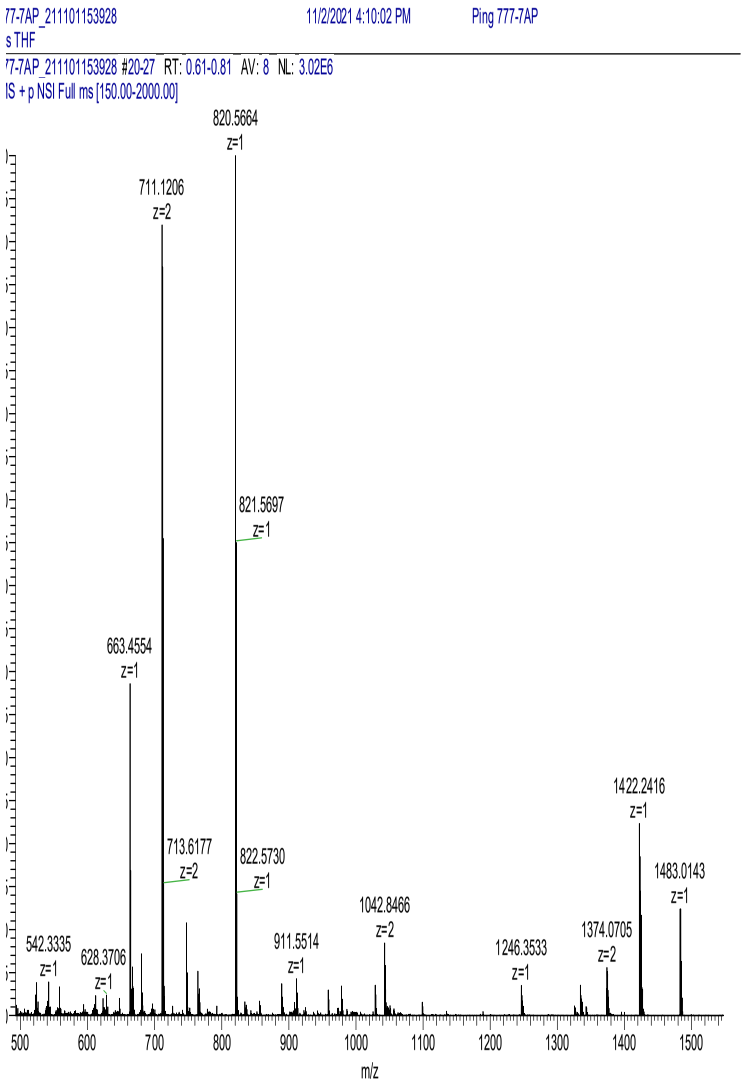
77-7AP_211101153928
11/2/2021 4:10:02 PM
Ping 777-7AP
s THF
77-7AP_211101153928 #20-27 RT: 0.61-0.81 AV: 8 NL: 3.02E6
IS + p NSI Full ms [150.00-2000.00]
820.5664
z=1
711.1206
z=2
821.5697
z=1
663.4554
z=1
713.6177
z=2
822.5730
z=1
1422.2416
z=1
1483.0143
z=1
1042.8466
z=2
1374.0705
z=2
542.3335
z=1
628.3706
z=1
911.5514
z=1
1246.3533
z=1
500
600
700
800
900
1000
1100
1200
1300
1400
1500
m/z

7-7AP_211101153928 11/2/2021 4:10:02 PM Ping 777-7AP
s THF
7-7AP_211101153928 #20-27 RT: 0.61-0.81 AV: 8 NL: 6.75E5
S + p NSI Full ms [150.00-2000.00]

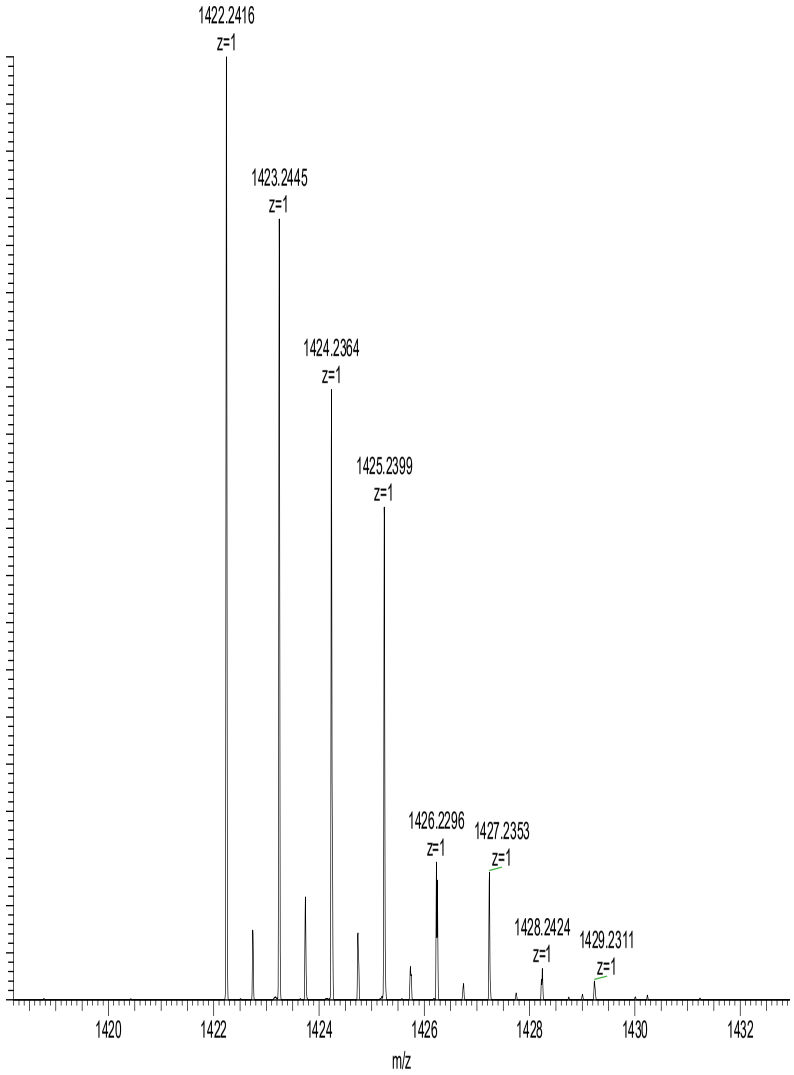

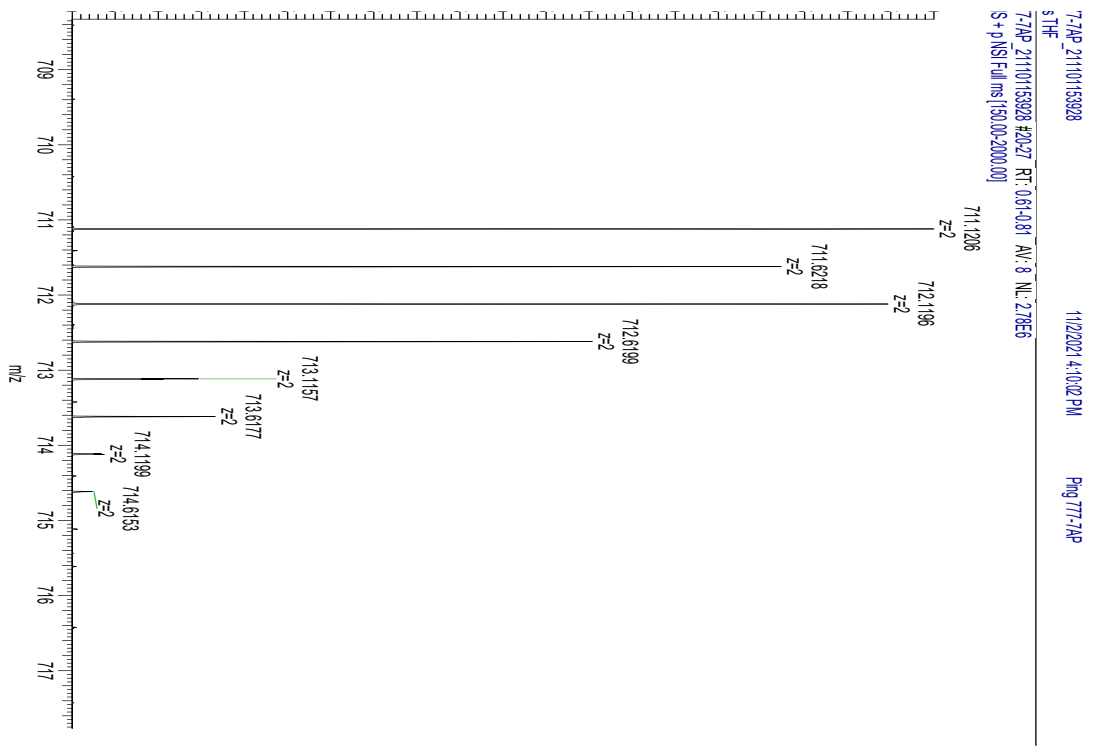

HR-MS spectrum of **TTF-TAP**.

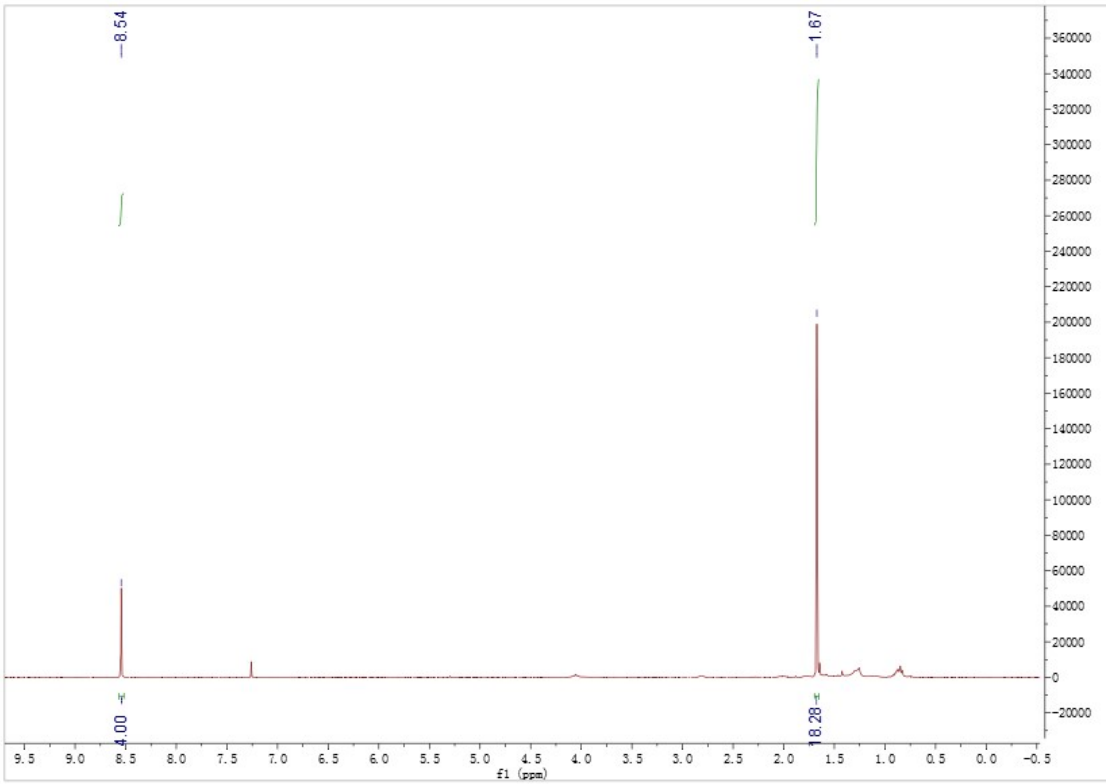

^{1}H NMR spectrum of ***t*-Bu-TAP** in $CDCl_3$.

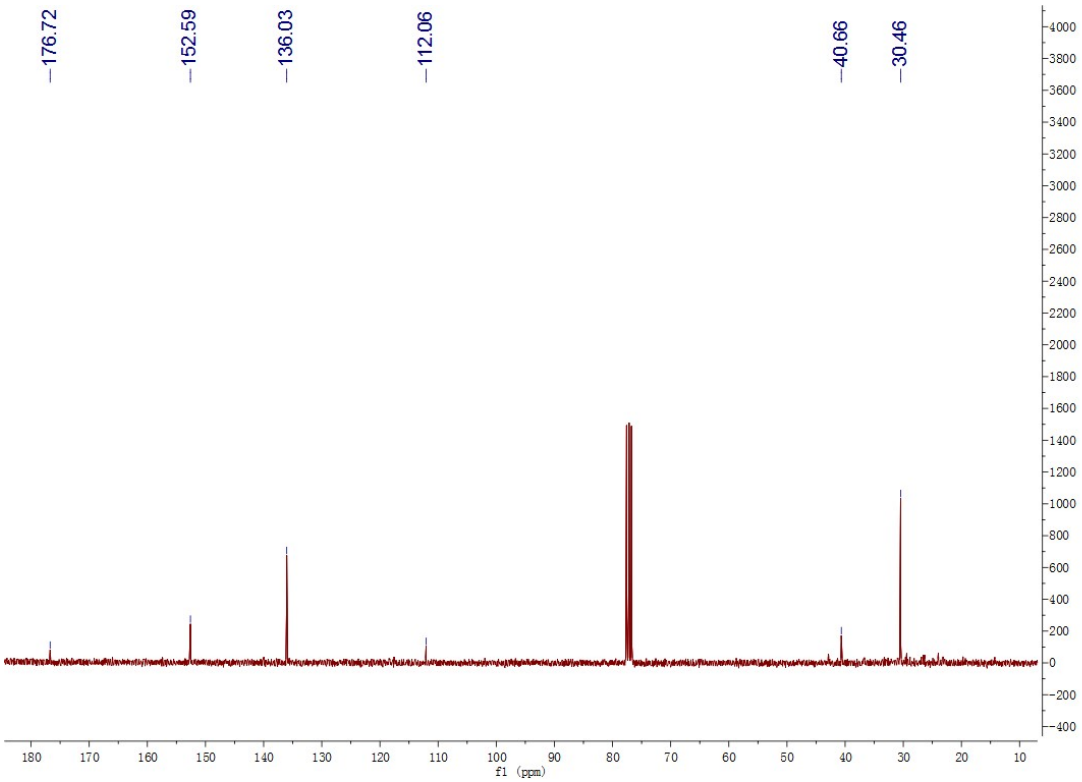

^{13}C NMR spectrum of ***t*-Bu-TAP** in $CDCl_3$.

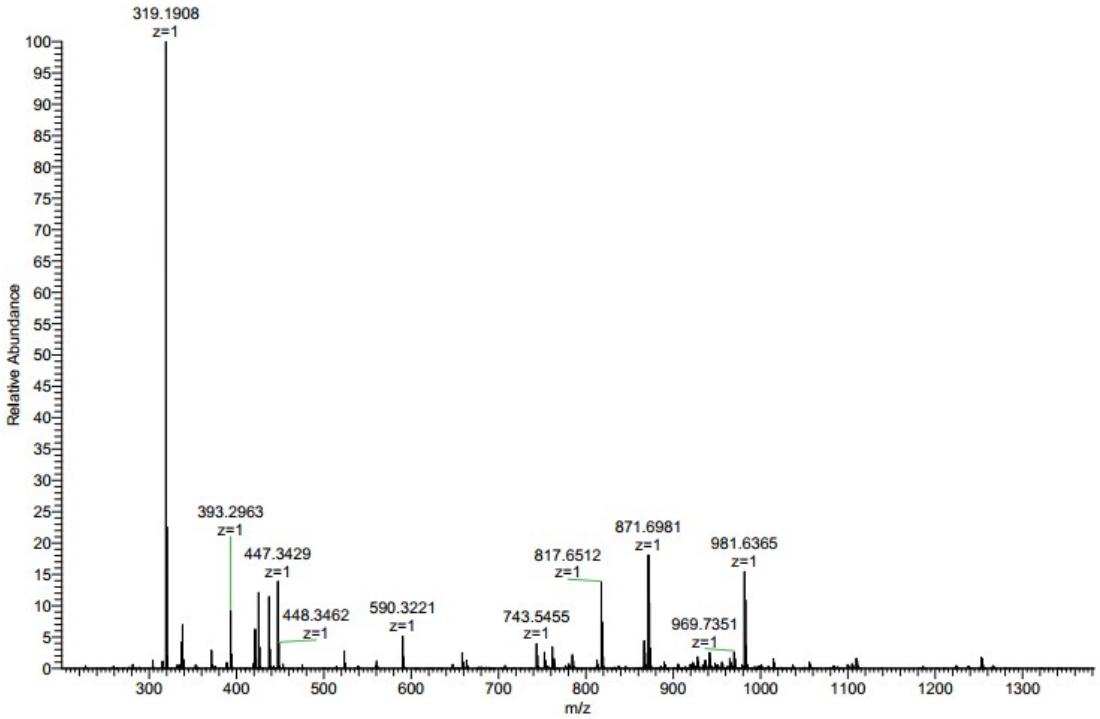

HR-MS spectrum of ***t*-Bu-TAP**.

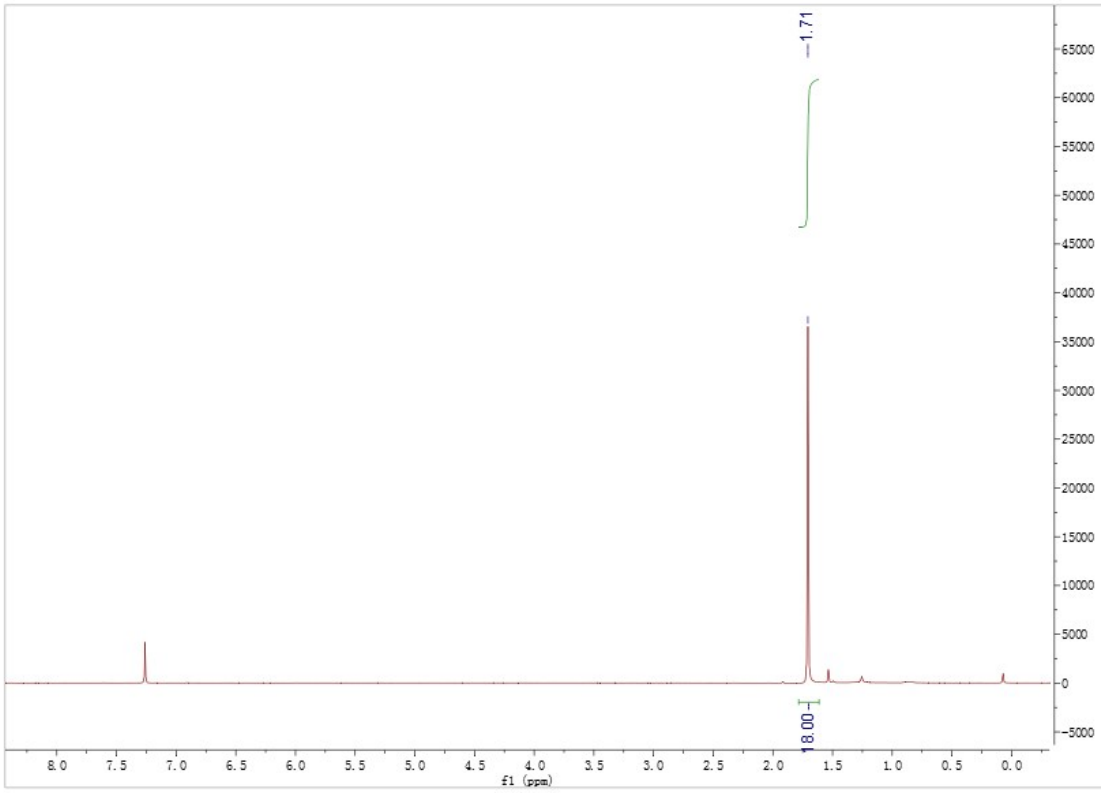

^{1}H NMR spectrum of **tetrabromo-*t*-Bu-TAP** in $CDCl_3$.

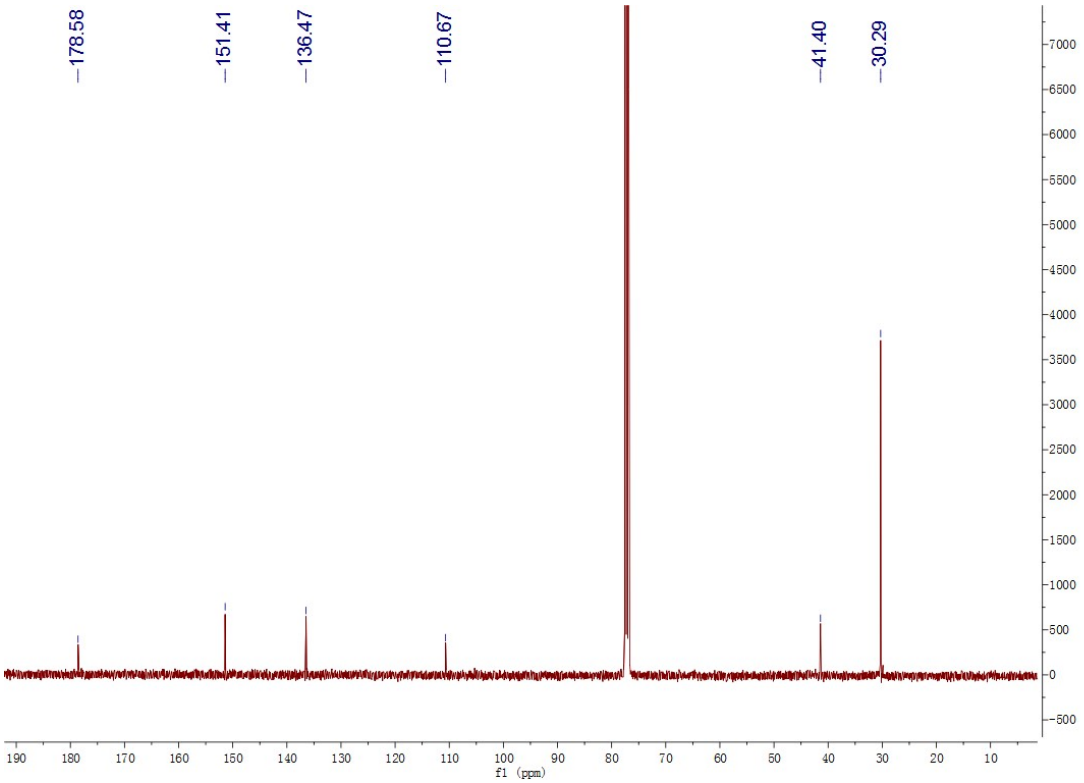

^{13}C NMR spectrum of **tetrabromo-*t*-Bu-TAP** in $CDCl_3$.

HR-MS spectrum of **tetrabromo-*t*-Bu-TAP**.

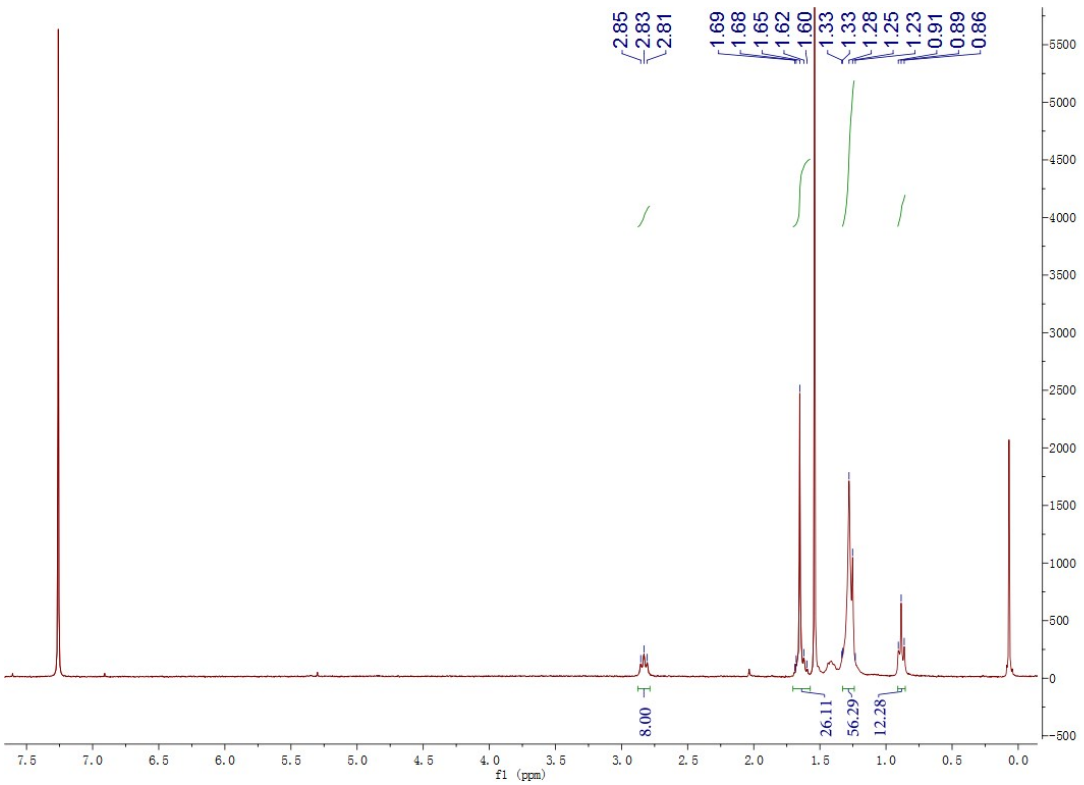

^{1}H NMR spectrum of **TTF-*t*-Bu-TAP** in $CDCl_3$.

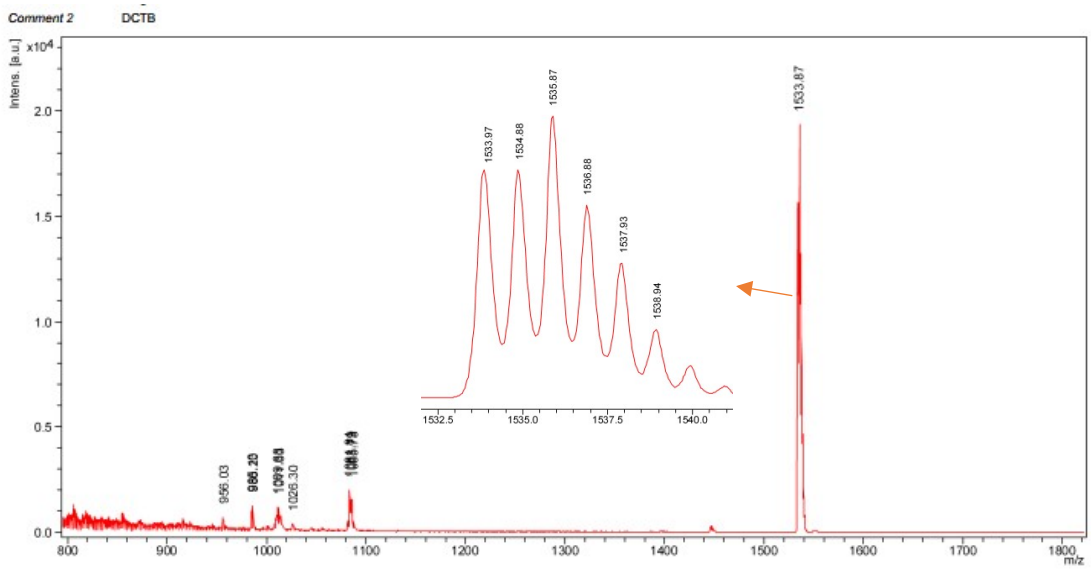

MALDI-TOF-MS analysis of **TTF-*t*-Bu-TAP.**

7F-tBu-7AP_211101153928 11/2/2021 4:19:32 PM Ping 77F-tBu-7AP
is THF

7F-tBu-7AP_211101153928 #75-79 RT: 2.48-2.59 AV: 5 NL: 7.44E5
MS + p NSI Full ms [150.00-2000.00]

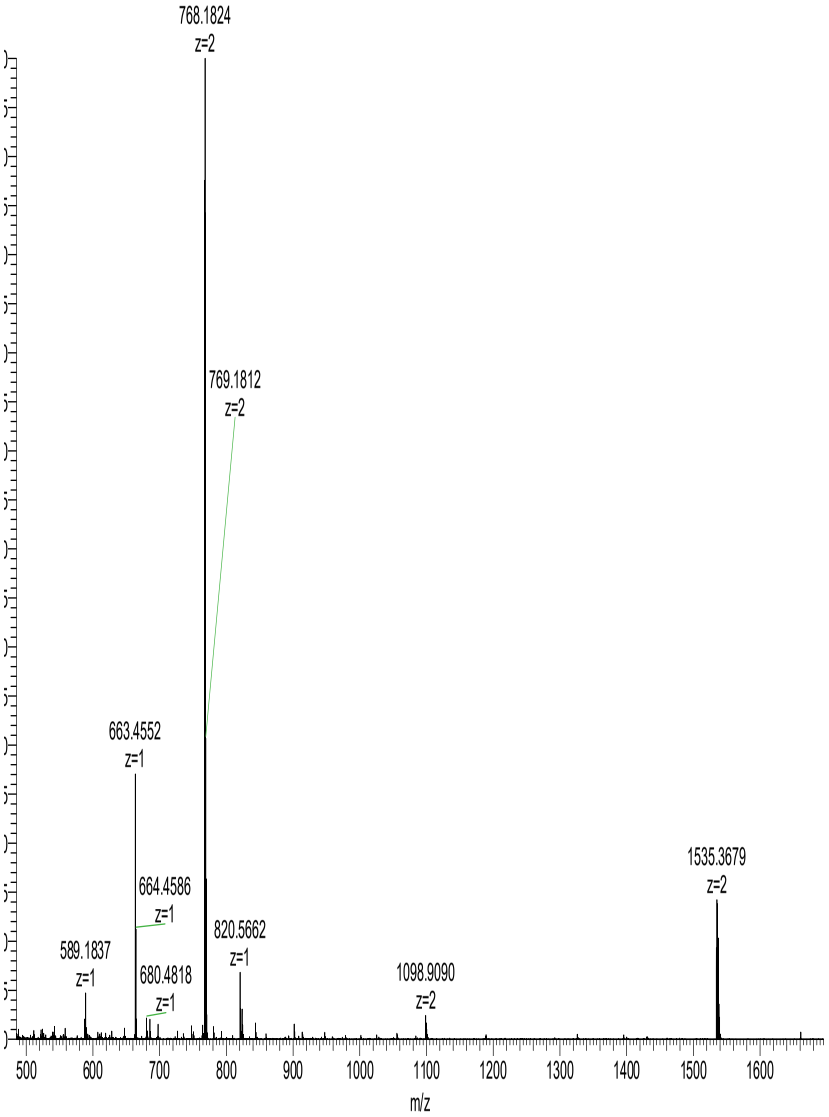

'F-tBu-7AP_211101153928 11/2/2021 4:19:32 PM Ping 77F-tBu-7AP
s THF
'F-tBu-7AP_211101153928 #75-79 RT: 2.48-2.59 AV: 5 NL: 1.06E5
S + p NSI Full ms [150.00-2000.00]

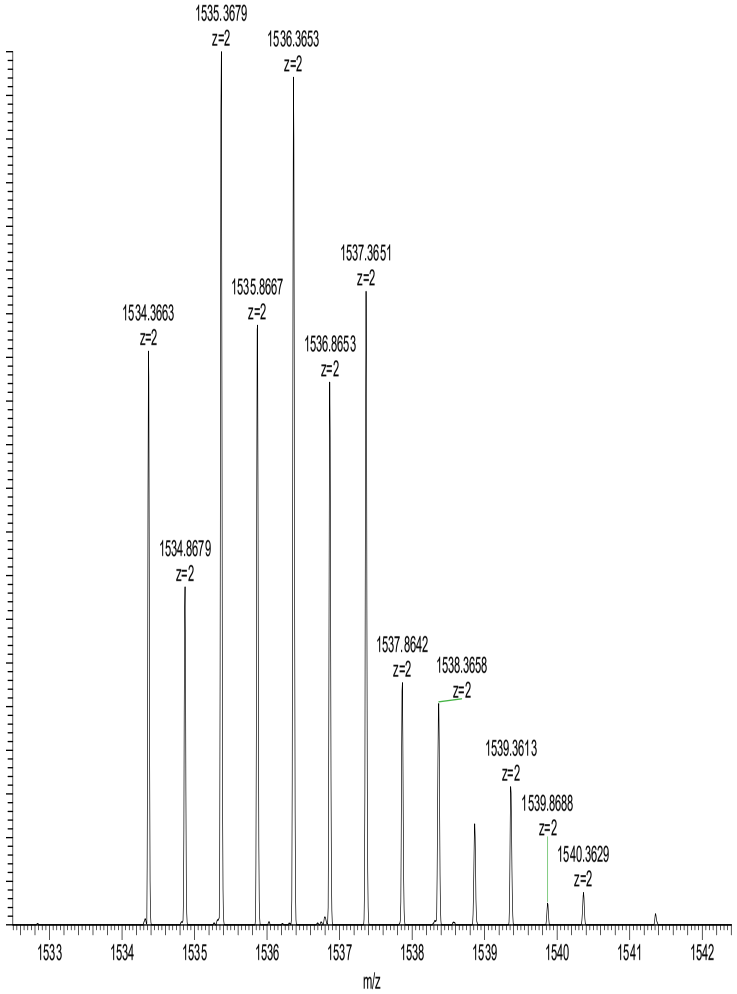

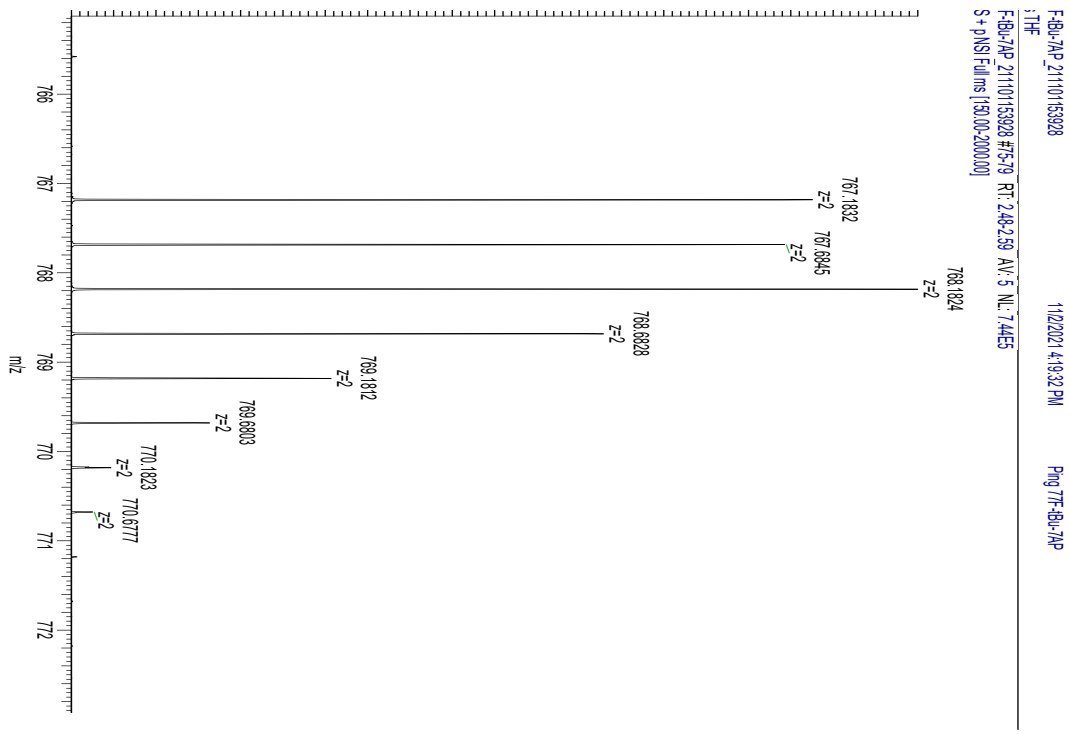

HR-MS spectrum of **TTF-*t*-Bu-TAP**.

References

1. V. Vitske, C. Konig, O. Hubner, E. Kaifer and H. J. Himmel, *Eur. J. Inorg. Chem.,* 2010, 115.
2. S. Geib, S. C. Martens, U. Zschieschang, F. Lombeck, H. Wadepohl, H. Klauk and L. H. Gade, *J. Org. Chem*., 2012, **77**, 6107.
3. A. V. Marenich, C. J. Cramer and D. G. Truhlar, *J. Phys. Chem. B*, 2009, **113**, 6378.